

Exoskeletal strength and cuticle composite profile of the acorn weevil rostrum

M. Andrew Jansen,^{1,*} Jason Williams,² Nikhilesh Chawla,² and Nico M. Franz¹

¹School of Life Sciences, Arizona State University, Tempe, AZ 85287, USA

²School for Engineering of Matter, Energy, and Transport,
Arizona State University, Tempe, AZ 85287, USA

(Dated: March 7, 2019)

The acorn weevil snout exhibits remarkable flexibility and toughness that are derived from the microarchitecture of its exoskeleton. Here we characterize modifications to the composite profile of the rostral cuticle that simultaneously enhance the flexibility and fracture toughness of the distal portion of the snout. Using Classical Laminate Plate Theory (CLPT) we estimate the effect of these modifications on the elastic behavior of the exoskeleton. Additionally, changes in the relative layer thicknesses and orientation angles of layers in the exoskeleton are related to the tensile behavior of the snout in six species of diverse morphology, and we demonstrate that a highly curved rostrum can be completely straightened without structural damage. We demonstrate that increased endocuticle thickness is strongly correlated with increased tensile strength in the snout. Consequently, snout stiffness is shown to be inversely correlated with fracture toughness. Finally, we identify exocuticle rich invaginations of the occipital sutures both as a likely site of crack initiation in tensile failure and as a source of morphological constraint on the evolution of the snout.

The exoskeleton of Coleoptera (beetles) is a hierarchically-structured fibrous composite characterized by variously arranged α -chitin (N-acetylglucosamine) nanofibrils embedded in a heterogeneous protein matrix [1–3]. Although α -chitin is brittle and strongly anisotropic, beetle cuticle is simultaneously rigid and tough due to its unique laminate microstructure (see kamp, vincent for review), which we characterize in detail below [4–6]. Impact-prone areas and exaggerated structures in arthropods generally exhibit cuticle organization that resists deformation and fracture (e.g. [7–11]); however, acorn weevils in the genus *Curculio* Linnaeus, 1758¹ instead exhibit unusual distal flexibility in an elongate extension of the head called the rostrum (snout) [1, 12–14]. The rostrum is a hollow, strongly curved (over 90° in some species), cylindrical, exoskeletal extension of the otherwise nearly-spherical head, which bears at its apex the terminal chewing mouthparts [14–18]. This structure is used by the female to feed and to excavate sites for egg-laying (oviposition, see Fig. 1), and can be repeatedly bent without evident damage despite being composed of the same material as other rigid body parts [1, 12–14]. By maintaining constant pressure on the snout and rotating around the bore-hole, females are able to flex the rostrum into a straightened configuration and produce a linear channel into the fruit; a single female may prepare hundreds of such sites as an adult [13, 19, 20].

While this behavior has been observed in many species

of *Curculio* [13, 14, 19, 20], it was unclear how the rostrum of female acorn weevils can withstand the repeated, often extreme bending incurred during the process of egg-chamber excavation. In this study we characterize the composite profile of the rostral cuticle to account for the observed flexibility of the snout. We show that the relative layer thicknesses and fiber orientation angles of the exocuticle and endocuticle of the rostrum are strongly differentiated from the head capsule and other body parts, and we estimate the effect of these differences on the elasticity of the cuticle using Classical Laminate Plate Theory (CLPT). Because recent studies have shown that the yield strength of the beetle exoskeleton is lower in tension than compression [22], we perform a comparative analysis of the ultimate tensile strength of the rostrum across species and snout morphotypes; we also report the results of displacement-controlled load cycling of the snout in a species with strongly curved morphology. We relate an observed increase in the volume fraction of endocuticle in the rostrum to higher tensile strength at the rostral apex in all tested species, and find that a strongly curved rostrum can be flexed repeatedly without harm to the structure.

We additionally describe the fracture mechanics of the snout and consider how modification of the cuticle may prevent crack formation during oviposition. Based on our findings, we posit that the composite profile of the rostral apex enables the snout to undergo repeated digital flexion while remaining within the elastic limits of the material, mitigating the risk of structural damage, and without evident alteration of the mechanical properties of the individual components of the cuticle across the structure and between species. Thus, the flexibility and tensile strength of the rostrum appear to be derived exclusively from modification of the composite architecture of the exoskeleton. To our knowledge, this is the first time that a modified composite profile has been reported as a means of enhancing structural elasticity in the insect

* corresponding author, email: majanse1@asu.edu

¹ Pursuant to the International Code of Zoological Nomenclature, the first mention of any specific epithet will include the full genus and species names as a binomen (two part name) followed by the author and date of publication of the name. This is not an in-line reference; it is a part of the name itself and refers to a particular species-concept as indicated in the description of the species by that author [21].

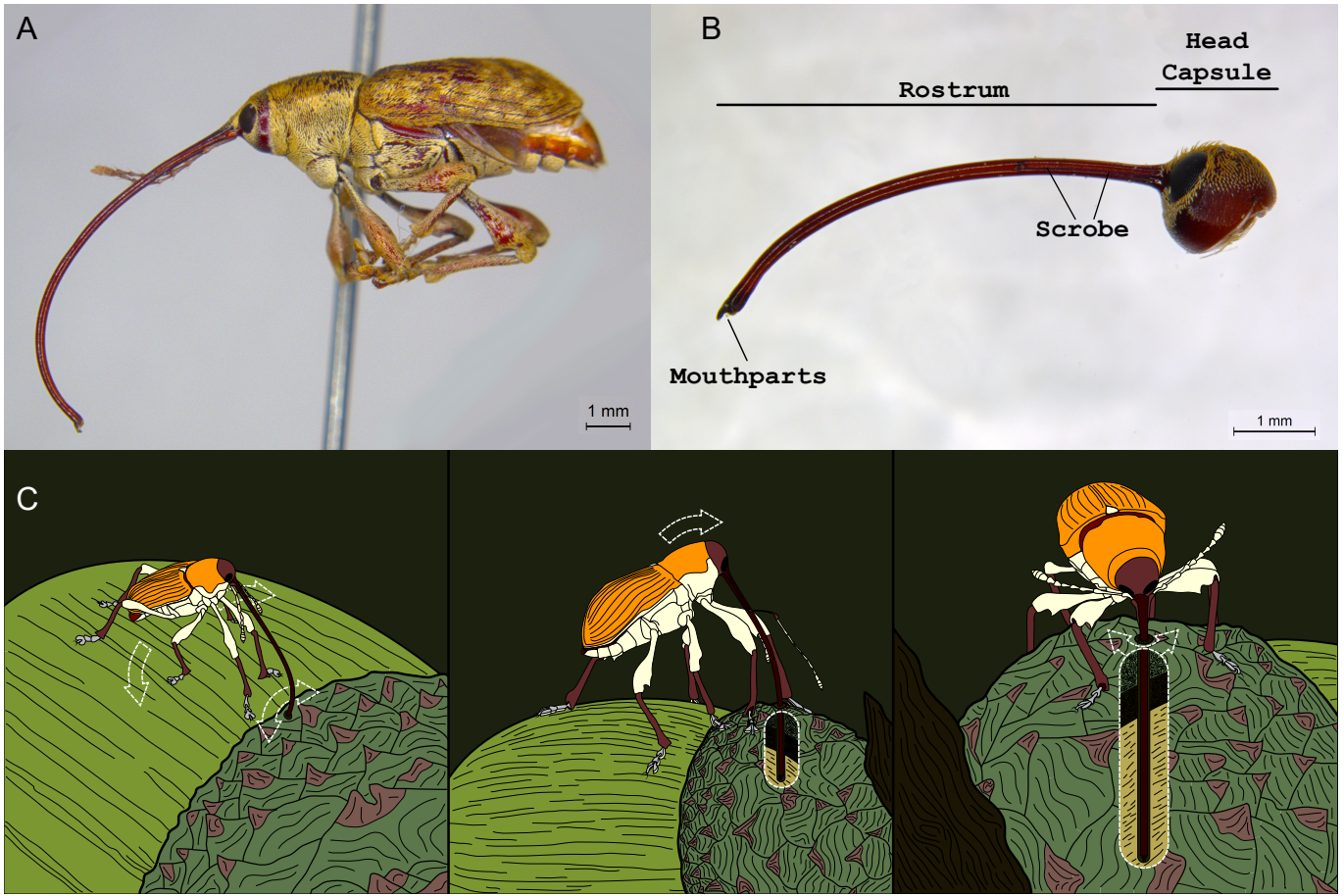


FIG. 1. Morphology and oviposition behavior of female *Curculio*. **a.** Lateral habitus image of female *Curculio sayi* ((Gyllenhal, 1836)) featuring the elongate, strongly curved rostrum. **b.** Lateral view of the head of a female specimen of *Curculio longinasus*, with major anatomical features indicated. **c.** Illustration of the oviposition behavior of female *Curculio*, proceeding from left to right: a female makes an incision in the host fruit, flexes the head directly over the bore hole using the front legs, then maintains tension on the snout while rotating to excavate a linear channel into the fruit. During this process, the rostrum is bent until completely straight.

⁷⁴ exoskeleton (but see [23]).

⁷⁵ I. MICROSTRUCTURE OF THE CURCULIO ⁷⁶ ROSTRUM

⁷⁷ In arthropods (including beetles), the exocuticle is
⁷⁸ comprised of numerous unidirectional laminae of chitin
⁷⁹ nanofibrils; each layer is the thickness of a single fiber
⁸⁰ (2-4 nm) embedded in a proteinaceous matrix [24, 25].
⁸¹ These layers are stacked at a more or less constant an-
⁸² gle to each other, forming a quasi-isotropic laminate
⁸³ known as the Bouligand structure [6, 26, 27]. This
⁸⁴ layout effectively mitigates the strong anisotropy of α -
⁸⁵ chitin to yield a versatile building material for the ex-
⁸⁶ oskeleton [2, 24, 25, 28]. Beetle endocuticle, how-
⁸⁷ ever, is unique among arthropods and is comprised of
⁸⁸ large (1-5 μm diameter in *Curculio*) unidirectional bun-
⁸⁹ dles of chitin, called macrofibers. Chitin macrofibers
⁹⁰ are orthotropic (axial: $E_1 = 8.5 \text{ GPa}$, transverse:

⁹¹ $E_2 = E_3 = 0.52 \text{ GPa}$ [1]) and arranged in unidirec-
⁹² tional plies, seen in Figs. 2, 3 [4, 5]. Typically, adjacent
⁹³ macrofiber laminae are paired and pseudo-orthogonal
⁹⁴ (i.e., angled approx. 90° to each other [29], see Fig. 3),
⁹⁵ with a constant stacking angle between pairs, although
⁹⁶ other configurations have been observed [3-5, 30]. This
⁹⁷ geometric sequence of the macrofiber laminae yields an
⁹⁸ approximately transversely isotropic composite, similar
⁹⁹ to the Bouligand structure [5, 25]. Notably, the result-
¹⁰⁰ ing laminate is less rigid than the exocuticle, but ex-
¹⁰¹ hibits greater toughness because the pseudo-orthogonal
¹⁰² plies effectively inhibit crack formation and propagation
¹⁰³ between successive layers [3-5].

¹⁰⁴ Serial thin sectioning and scanning electron microscopy
¹⁰⁵ of fractured *Curculio* specimens revealed that endocu-
¹⁰⁶ ticle in the head capsule fits this general profile, with
¹⁰⁷ an angle of approximately 30° between successive pairs
¹⁰⁸ of pseudo-orthogonal plies. Additionally, in the head
¹⁰⁹ capsule, the thickness of the exocuticle and endocu-
¹¹⁰ ticle in cross section are nearly equal (typically between

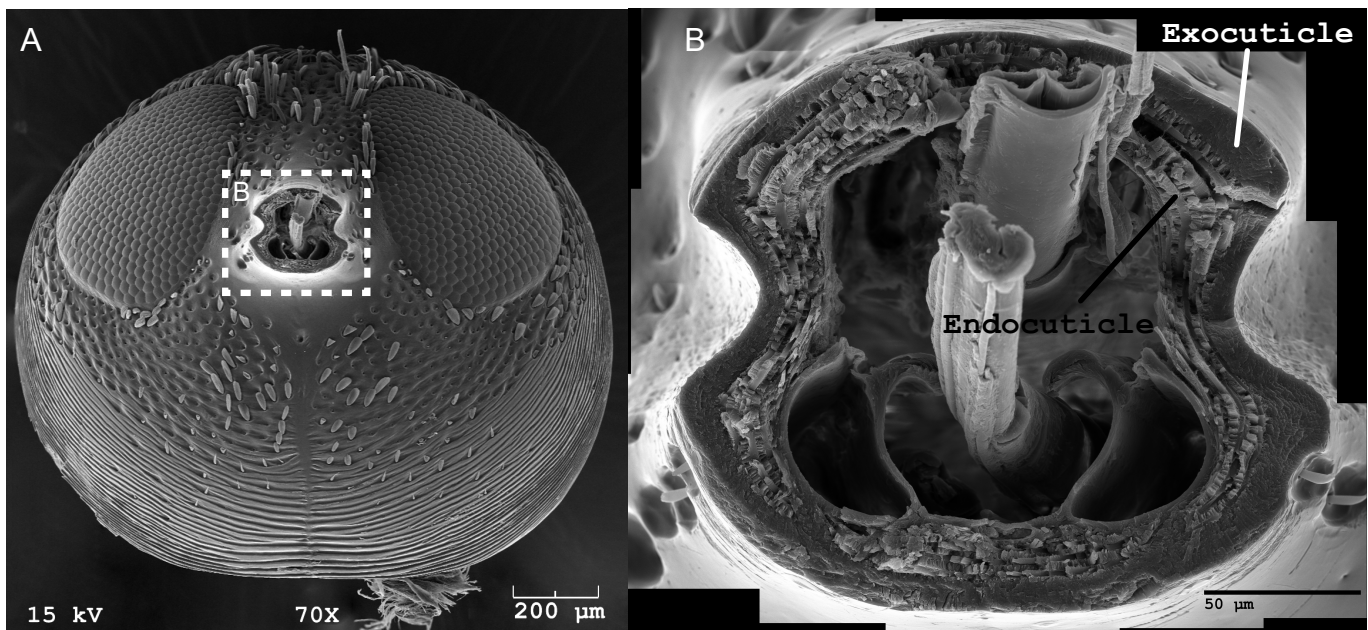


FIG. 2. Gross divisions of cuticle in the rostrum. **a**, Scanning electron micrograph of the head capsule, in frontal view, of female *Curculio sulcatus* (Casey, 1897), with the rostrum removed. **b**, Magnified view of the junction between the rostrum and head capsule showing the division of the cuticle into two general regions: the exocuticle and the endocuticle.

111 20–30 μm). However, we found that the cuticle compos-
112 ite lay-up of the rostral apex is strongly differentiated
113 from the head capsule (Fig. 3). Distally the exocuticle
114 is reduced to a thin shell (ca. 5 μm), with the endocu-
115 ticle thickened to offset this reduction and maintain a
116 constant cuticle thickness (ca. 50 μm total) throughout
117 its length. Moreover, the endocuticular macrofibers ex-
118 hibit no rotation between successive pseudo-orthogonal
119 plies, and are oriented at approximately $\pm 45^\circ$ to the lon-
120 gitudinal axis of the snout (i.e., an antisymmetric [$\pm 45^\circ$]
121 angle-ply laminate). We previously identified these mod-
122 ifications to the composite structure of the cuticle within
123 a single species, *C. longinasus* Chittenden, 1927 [1, 12];
124 however this composite profile has now been uncovered in
125 the rostrum of six additional, phylogenetically disparate,
126 species (detailed in methods), indicating that this is likely
127 a genus-wide trait. In all examined species, the portion
128 of the snout between the head capsule and apex of the
129 scrobe exhibits a gradual transition in composite profile
130 along an anterior-posterior gradient.

131 We estimated the effect of differential cuticle orga-
132 nization on uni-axial membrane and transverse-flexural
133 Young's moduli of the cuticle in the rostral apex and
134 head capsule using Classical Laminate Plate Theory
135 (CLPT), as detailed in our methods [31, 32]. The ef-
136 fective elastic constants of the cuticle regions of *C. longi-*
137 *nasus* (estimated previously, see [1]) were used to con-
138 struct constitutive equations for the entire cuticle of
139 that species. The cuticle of the head capsule was
140 estimated to have membrane and flexural moduli of
141 $E_m = 4.77 \text{ GPa}$ and $E_f = 6.04 \text{ GPa}$, respectively;
142 however, in the rostral apex we found that these values

143 were reduced by approximately 72% and 60%, respec-
144 tively ($E_m = 1.36 \text{ GPa}$, $E_f = 2.44 \text{ GPa}$). Two hypo-
145 thetical cuticle lay-ups were also modeled to individually
146 assess the contributions of either modified layer thickness
147 or stacking angle sequence to cuticle flexibility. The ef-
148 fective moduli of a configuration with the angle stacking
149 sequence of typical cuticle (i.e., in the head capsule) but
150 possessing the layer thicknesses of the rostral apex were
151 calculated as $E_m = 3.73 \text{ GPa}$, $E_f = 4.31 \text{ GPa}$, repre-
152 senting 22% and 29% decreases from unmodified cuticle,
153 respectively. Similarly, a hypothetical cuticle with the
154 layer thicknesses of ordinary cuticle but possessing the
155 angle stacking sequence of the rostral apex (i.e., $\pm 45^\circ$
156 angle-ply in the endocuticle) had effective elastic moduli
157 of $E_m = 3.77 \text{ GPa}$, $E_f = 5.76 \text{ GPa}$, representing 21%
158 and 4.7% decreases from unmodified cuticle, respectively.
159 Each of the cuticle modifications noted in the rostral apex
160 individually decreased the elastic moduli of the cuticle;
161 however, they appear to have a synergistic combined ef-
162 fect on cuticle elasticity, rather than a simple additive
163 effect. This result suggests that both modifications are
164 necessary in order for the snout to function properly in
165 the living animal, where the combined effect allows the
166 rostrum to bend until completely straight without frac-
167 ture.

II. FORCE-CONTROLLED LOADING TO FRACTURE

168 To better characterize the failure behavior of the ros-
169 trum, we performed tensile testing on the snouts of six

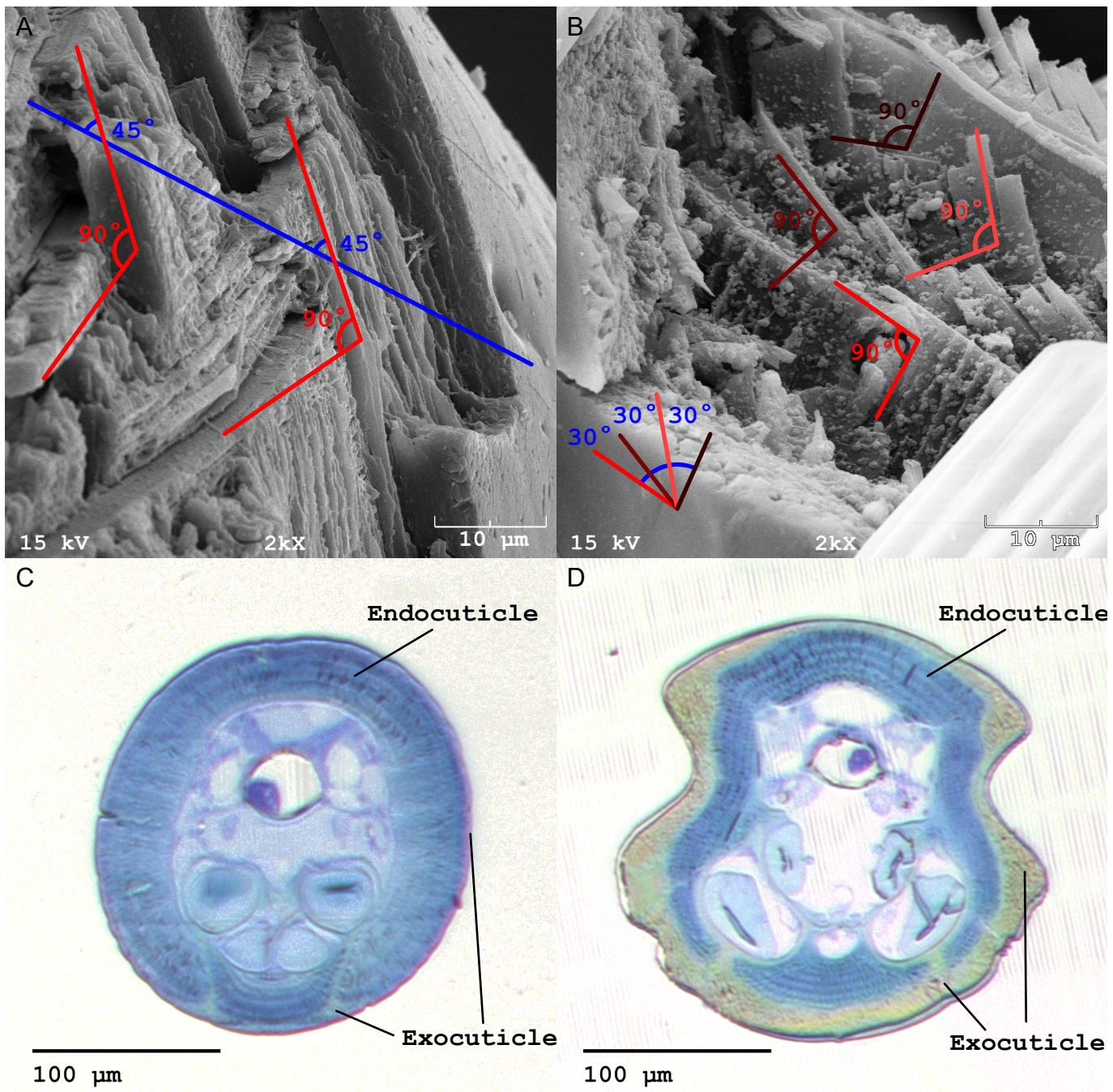


FIG. 3. Composite profiles of rostral cuticle. **a**, Scanning electron micrograph of a fractured specimen of *Curculio humeralis* (Casey, 1897), showing that the cuticle of the rostral apex is organized as a $\pm 45^\circ$ angle-ply laminate.. **b**, Scanning electron micrograph of a fractured specimen of *Curculio caryae* (Horn, 1873), showing that the cuticle of the rostral base and head capsule has a roughly 30° stacking angle between each pair of pseudo-orthogonal plies. Semi-thin sections of cuticle from a specimen of *C. humeralis*, stained with toluidine-blue-borax, demonstrating: **(c)** that the exocuticle of the rostral apex is reduced to a thin shell close to $5\text{ }\mu\text{m}$ thick, with the endocuticle thickened to maintain a constant laminate thickness; and, **(d)** that the exocuticle of the head capsule and base of the snout occupies nearly half of the through-thickness of the cuticle.

172 *Curculio* species that representing a mixture of closely 176 controlled, uniaxial loading to fracture at a constant
 173 and distantly related taxa (see Methods) [33–36]. Each 177 stress rate of $1.0\text{ gf}\cdot\text{s}^{-1}$ (detailed in Methods). In gen-
 174 specimen was immersed in di-H₂O for 24 hours, to sim- 178 eral, the specimens exhibited a non-linear viscoelastic re-
 175 ulate the living tissue (see [37]), then subjected to force- 179 sponse curve characterized by a sharp increase in stress

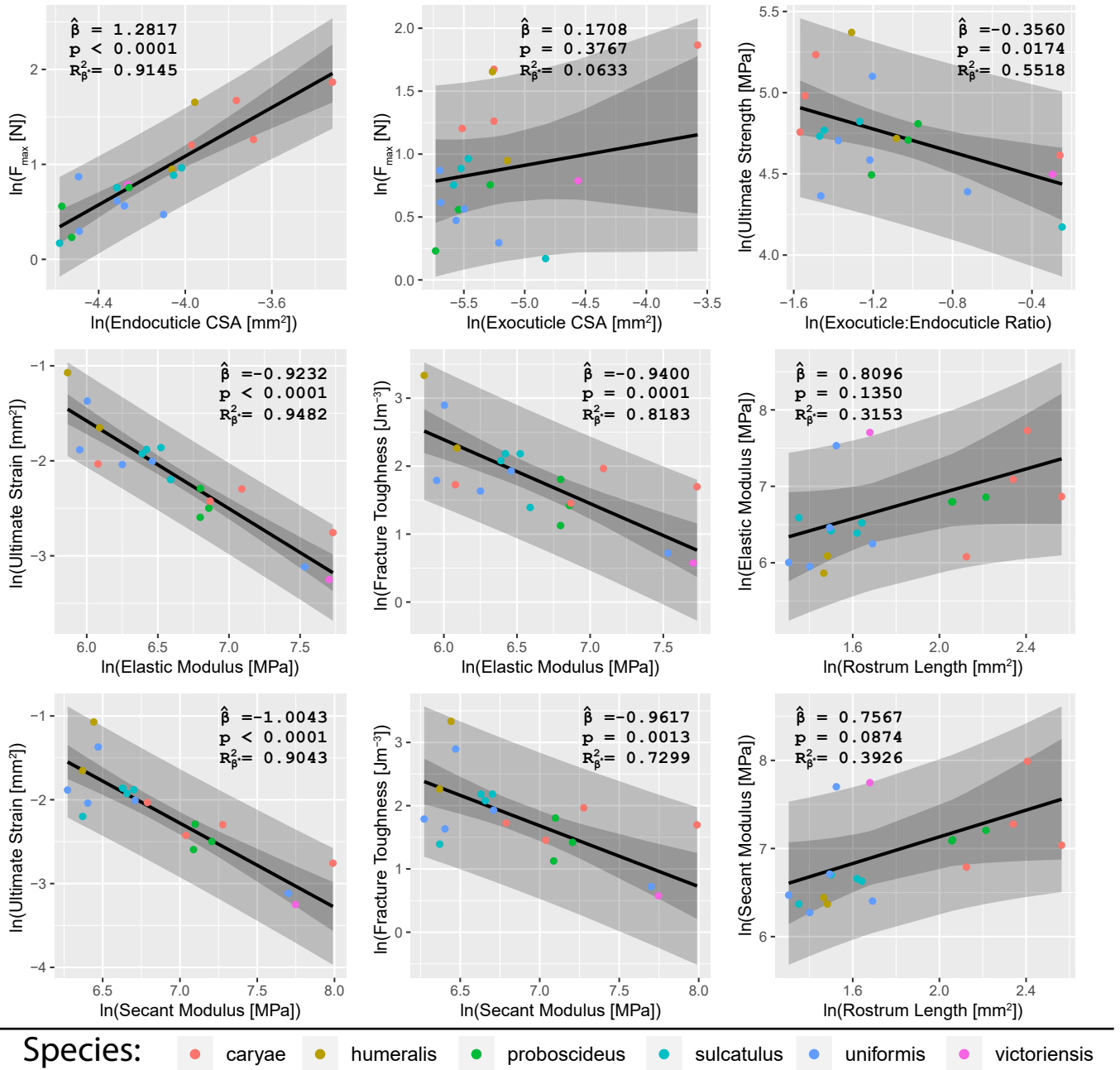


FIG. 4. Tensile properties of the *Curculio* rostrum. Each plot shows the relationship between two variables as predicted by a phylogenetic linear mixed-effect model, with species as a random effect and a variance-covariance matrix generated from Brownian motion over the preferred phylogeny of Bonal et al. [34]. The gray regions represent the prediction interval and bootstrapped 95% confidence interval of the model. The estimated fixed effect $\hat{\beta}$ is given, along with the p-value of a t-test assessing whether $\hat{\beta}$ is significantly different from zero. Also reported is a generalized marginal R_{β}^2 for assessing fixed effects (see online Methods for more information). In general, we find that increased endocuticle thickness is associated with greater tensile strength, and that stiffness is inversely correlated with toughness.

at higher strains, terminating in brittle fracture [38]. We postulate that strain hardening occurs as the longitudinal axis of the macrofibers becomes more closely aligned to the cylindrical axis of the rostrum, thereby resisting tension more directly with increasing strain [39].

We examined the correspondence between composite

structure and mechanical behavior of the snout using phylogenetic linear mixed effects models (PGLM, Fig. 4) to account for phylogenetic non-independence in residual variance, with species membership included as a random effect [40, 41]. Our models show that the maximum force sustained at the site of failure was strongly

correlated with the cross-sectional area of the endocuticle ($\hat{\beta} = 1.28, p < 0.0001$), and not the exocuticle ($\hat{\beta} = 0.17, p = 0.38$), at that site. Accordingly, there was a negative correlation between ultimate tensile strength of the specimen and the ratio of exocuticle to endocuticle cross-sectional area at the site of fracture ($\hat{\beta} = -0.36, p = 0.017$). Although CLPT predicts a positive association between the proportion of exocuticle and stiffness of a generalized cuticle, we found no evidence of correspondence between the cross-sectional properties of the fracture site and the gross behavior of the entire rostrum. Because the cross-sectional areas of the cuticle regions vary across the length of the head along an anterior-posterior gradient, it is not possible to correlate measurements from the fracture surface to the properties of the entire snout.

Instead, we found that the uniaxial elastic modulus (low strain: E_{low}) and secant modulus at failure (E_{sec}) were inversely correlated with ultimate strain and fracture toughness (see Fig. 4), implying that stiffer specimens, and by extension, stiffer cuticle profiles, are generally more brittle. We also observed a moderate, but not statistically significant, stiffening size-effect with respect to rostral length, contrary to our expectation that a longer, more strongly curved (see [35, 36]) snout would require increased flexibility to avoid fracture during oviposition. One possible explanation for this trend might be that longer snouts have a longer transition gradient from basal to apical profile to reinforce the junction between the rostrum and head capsule against buckling. Thus, Young's modulus of the rostrum would be comparatively higher in these species because of the higher volume fraction of exocuticle. From these tests, we infer that the gross elastic behavior of the cuticle is consistent across the genus, and that a single mechanism (i.e. the modified composite profile) confers increased flexibility and tensile strength to the rostral apex in the genus *Curculio*. In addition, the endocuticle demonstrably contributes more to rostral tensile strength than the exocuticle, likely because of its organization into large bundles of aligned, anisotropic fibers, leading to a trade-off between rigidity and toughness. Consequently, the altered composite profile of the cuticle in the rostral apex makes the rostrum simultaneously more flexible and fracture resistant.

III. LOAD CYCLING OF CURCULIO CARYAE

To confirm that repeated, proscribed straightening of the rostrum does not result in damage to the cuticle, we performed displacement-controlled fatigue testing on a typical female specimen of *Curculio caryae*, a species that exhibits extreme (80–90°, Fig. 5) rostral curvature [14, 19]. The specimen was aligned so that uniaxial tension would induce elongation of the distal portion of the rostrum with minimal off-axis deflection of the un-curved section. The strain per cycle was fixed at an amplitude

sufficient to completely elongate the snout and generate a tensile load of 1.0 N in the straightened configuration (ca. 20% ultimate strength) at a frequency of 0.33 Hz. The test was terminated after a period of two weeks (ca. 400K cycles) when the stress amplitude appeared to reach an asymptotic minimum. The rostrum behaved viscoelastically, indicated by hysteresis in the stress-strain relationship during each cycle. Strain amplitude decreased logarithmically with cycle number, and the specimen initially appeared to have deformed plastically during the test. We believed that this indicated damage to the specimen; however, after cleaning the specimen in a 24 hour wash with ethanol and water, we observed that rostrum returned to its original shape (Fig. 5).

We cannot fully account for the stress relaxation of the rostrum after testing, but we speculate that it arose from the general mechanism associated with cuticle viscoelasticity. The endocuticle is made of aligned α -chitin nanofibrils whose crystalline structure is enforced by hydrogen bonds between individual chitin chains and with the protein matrix along their length; macroscopic viscoelastic behavior results from slippage between these chains in response to shearing between the chitin molecules [2, 42, 43]. We posit that repeated strain may have caused such slippage in the endocuticle of the rostral apex during the fatigue test; however, without sufficient time for the material to completely relax after deformation, the specimen would slowly accumulate strain and deform viscoelastically [39]. After immersion in ethanol and water, the cuticle would be sufficiently plasticized to allow the specimen to return to its original configuration, dissipating the accumulated strain.

The specimen did not show any evidence of fractures, micro-tears, or shear cusps anywhere in the surface of the exocuticle, and, furthermore, the tensile strength of the specimen was consistent with other members of its species ($F_{max} = 5.02$ N). Given this surprising result, it appears that the specimen was undamaged by the testing. We therefore expect that under normal conditions in life, repeated bending of the snout does not exceed the yield strength of the cuticle.

IV. FRACTOGRAPHY OF TEST SPECIMENS

Although it was not always possible to identify void nucleation and crack initiation sites given the complex failure modes evident in the fractured specimens, we observed several patterns characteristic of both the micro-scale behavior of the cuticle and the meso-scale behavior of the rostrum during uniaxial tensile failure (Fig. 6), which we describe here.

In transverse view, the exocuticle consistently presented a nearly continuous fracture surface, characteristic of comparatively brittle failure, presumably due to the relatively homogeneous arrangement of α -chitin lamellae in the Bouligand structure [24, 25]. The exocuticle typically appeared to fracture at lower strains than the

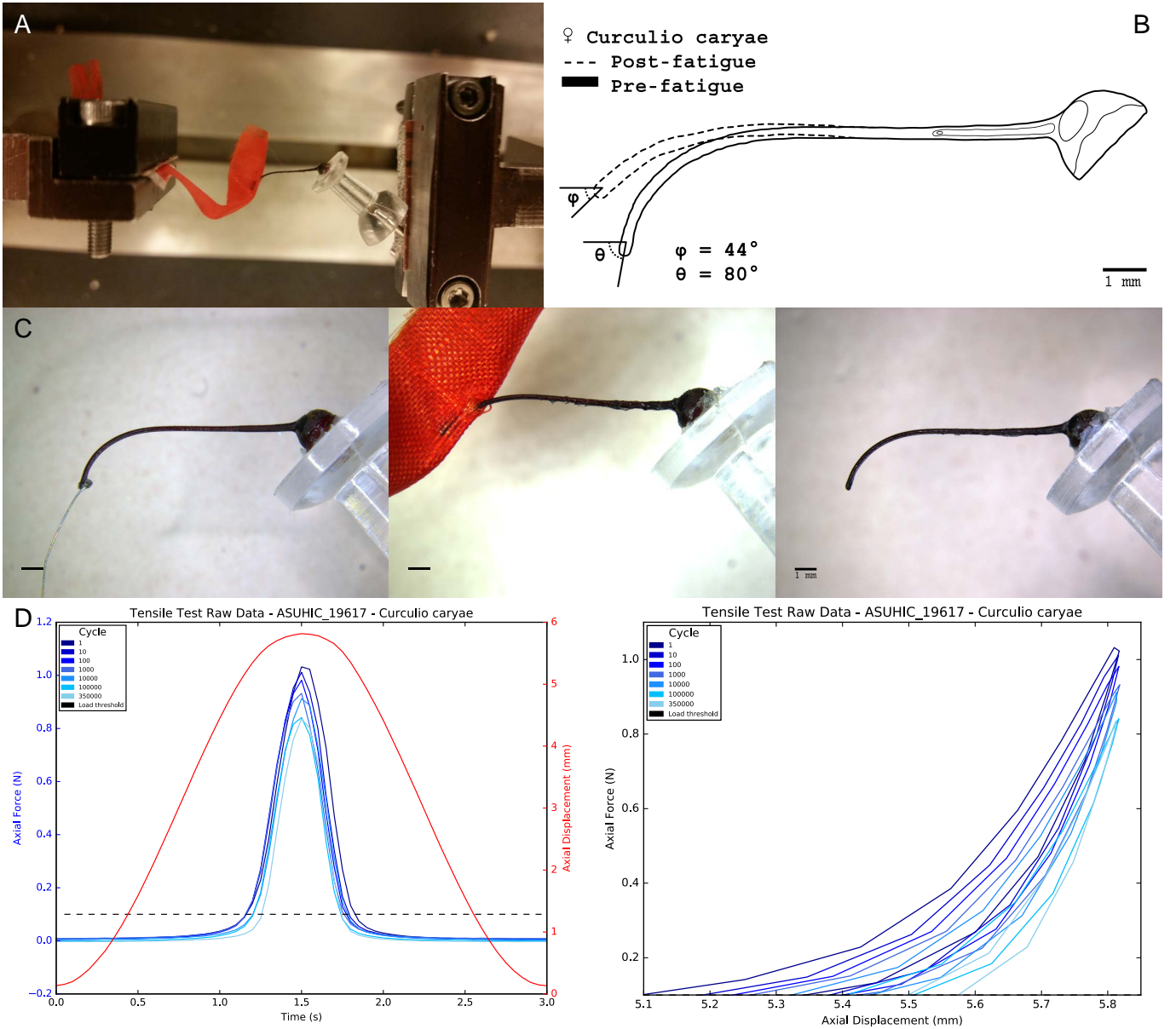


FIG. 5. Fatigue testing of a female *C. caryae*. **a**, Shows the fatigue testing setup, wherein the head capsule was fixed to a pedestal and the rostrum was attached to a strip of rip-stop nylon fabric using cyanoacrylate adhesive. The specimen was loaded in tension, and not compression, isolating the effect of tension on the fatigue behavior of the rostrum. **b**, An overlay of the pre- and post-fatigue states of the head show a clear effect from repeated protracted strain; however, **c**, Demonstrates that this effect is apparently not permanent. The first two panels to the left correspond to the pre- and post-fatigue states of the rostrum, respectively, but the third panel shows that the head has returned to its original shape after 24 hours soaking in a water/ethanol mixture. **d**, The two plots presented here are the raw force and displacement data from the fatigue test. The plot on the right shows clear viscoelastic behavior, indicated by hysteresis in the stress-strain response of the specimen, and exhibits a logarithmic decrease stress amplitude over time.

302 endocuticle, with shear-cusp formation evident both at
303 the fracture surface and across exocuticle adjacent to the
304 plane of fracture [44]. Conversely, the endocuticle exhib-
305 ited severe delamination, off-axis ply-splitting, and fiber-
306 pulling away from the fracture surface, indicating the
307 relatively high toughness of the unidirectional α -chitin
308 organization within the macrofibers [4, 5]. Because the

309 exocuticle of weevils is anchored to the endocuticle by
310 cross-linking fibers (see [5, 22]), exocuticular shear-cusp
311 formation in uniaxial tension suggests extension-shear
312 coupling within individual endocuticle laminae, implying
313 that ply-splitting occurred via mode II fracture between
314 macrofibers at high strain [31, 32]. We hypothesize that
315 intra-lamellar extension-shear coupling also yielded off-

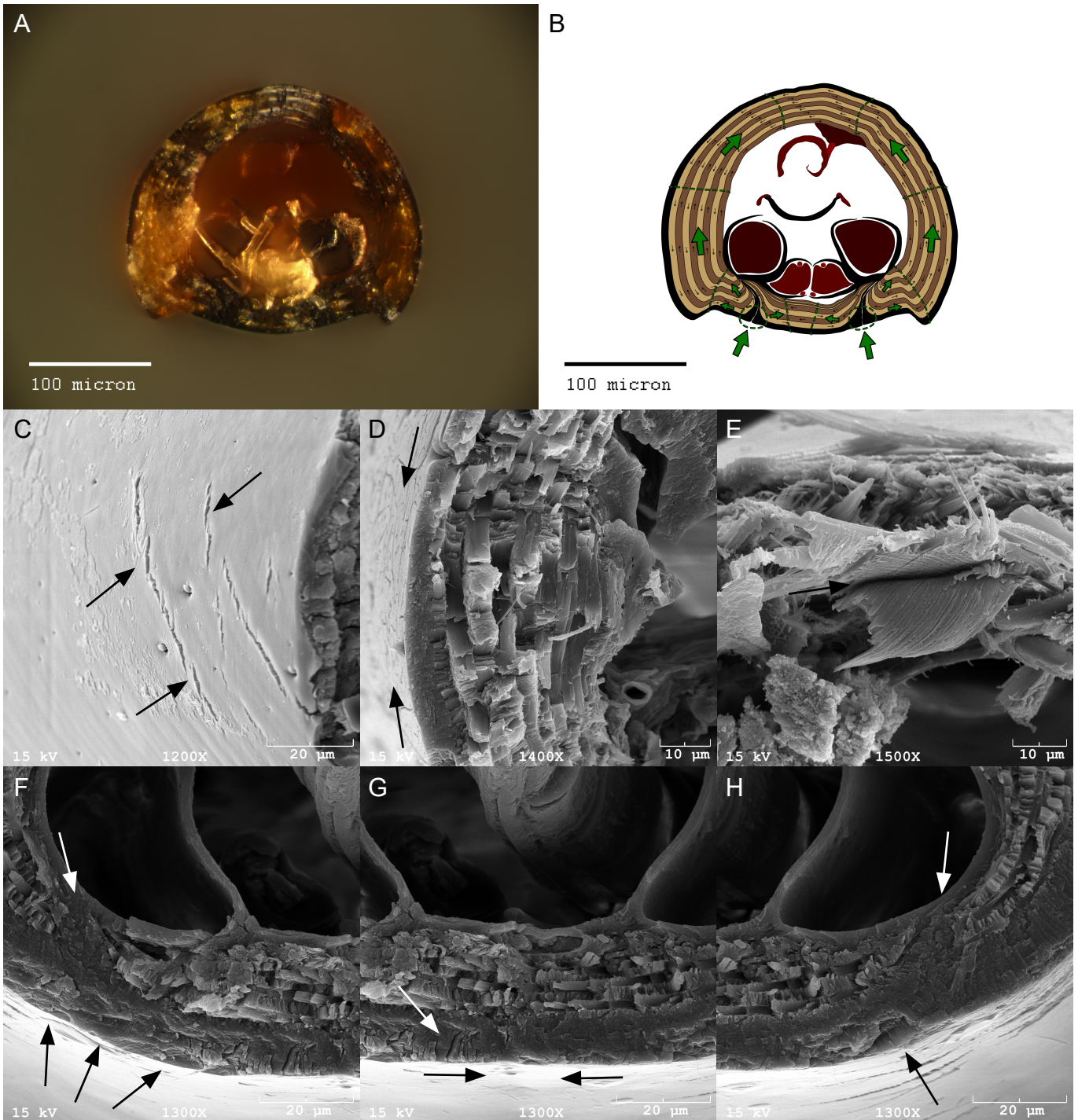


FIG. 6. Fractography of the *Curculio* rostrum. **a**, Light micrograph showing the fracture surface of a tensile tested rostrum, in the species *C. caryae*, exhibiting a typical failure mode, illustrated in **(b)**. The small, black arrows indicate the winding direction of the macrofiber lamina; green arrows and dotted lines indicate the direction of crack. Scanning electron micrographs highlight: **(c)** shear cusp formation, **(d)** tensile failure and off-axis macrofiber fiber-pulling, **(e)** interlaminar delamination, **(f,h)**, crack formation near invaginated exocuticle **(g)** ventral crack-front coalescence and shear cusp formation.

316 axis, in-plane resultant forces as a function of lamina ori- 320 macrofiber laminae would ultimately occur via mixed-
317 entation angle; mode III shearing then occurred between 321 mode I/II (transverse tension/intra-laminar shear) frac-
318 laminae with opposing in-plane resultant forces, causing 322 ture due to an increase in applied stress caused by ply-
319 the observed inter-ply delamination. Tensile failure of the 323 splitting in adjacent laminae [44].

At the meso-scale, most specimens fractured along a single plane across and between the occipital sulci, which are cuticle invaginations that traverse the entire length of the rostrum [15, 45]. These sulci increase the volume fraction of exocuticle in the ventral part of the snout and contain large interfaces ideal for void nucleation (see Fig. 6). The exocuticle of the occipital sulci usually displayed shear cusps oriented outward from the center of the invagination, continuing dorsolaterally and ventromedially. Ventrally the cusps converged toward a prominent scarp where the crack fronts joined, although in specimens with large cross-sectional areas of endocuticle, this was often obscured by delaminated endocuticular macrofibers.

The first layer of endocuticle usually fractured along the same plane as the exocuticle, and ventrally the endocuticle laminae typically converged toward a scarp-like region characterized by severe delamination and numerous de-bonded macrofibers. Additionally, macrofibers aligned with the direction of crack propagation exhibited extensive ply-splitting with intermittent transverse shearing, while macrofibers oriented against the direction of crack propagation primarily displayed fracture by transverse shear along the plane of ply-splitting in adjacent laminae. Because the laminae form a cylinder, contralateral fibers in the same lamina display opposing fracture modes. In addition, the ventrolateral surfaces often exhibited extensive inter-ply delamination and fiber de-bonding in scarp-like prominences, likely due to a combination of tensile failure and shearing along the dorsally-radiating crack front. Dorsally, the coalescent crack fronts often caused significant de-bonding and ply-splitting followed by broom-like tensile failure; in some specimens, the contralateral crack fronts were out of plane and coalesced via transverse shear through a large dorsal section of cuticle.

From these patterns we hypothesize that the exocuticle-rich occipital sulci are the most likely site for the initiation of void nucleation and catastrophic failure of the integrated rostral cuticle in cross section, as illustrated in Fig REF. According to this model, structural failure would take place as cracks propagate through the endocuticle from these sutures, which penetrate the entire thickness of the laminate [45]. Although other, more complex failure modes have been observed, we posit that in live specimens this is the most likely mechanism of tensile failure because typical bending behavior generates tension only along the ventral surface of the rostrum.

V. CONCLUSIONS

The rostrum of *Curculio* is characterized by a discontinuous composite profile, wherein the cuticle is strongly differentiated in terms of relative layer thicknesses and orientation angles along an anterior-posterior gradient. These modifications are sufficient to achieve marked reduction in the effective membrane and flexural moduli of the cuticle (72% and 60%, respectively) in constitu-

tive models based on CLPT, thereby accounting for the observed flexibility of the rostral apex in live specimens. However, these reductions can only be realized with both modifications to the cuticle, which have a non-additive effect on cuticle elasticity, implying that these weevils require both modifications to function properly during oviposition. Likewise, tensile and fatigue testing have revealed a trade-off between stiffness and fracture resistance (as measured by ultimate strain and toughness), mediated by the relative proportion of endocuticle in the laminate. The altered composite profile of the cuticle in the rostral apex makes the rostrum simultaneously more flexible and fracture resistant, permitting the structure to be flexed without exceeding the elastic limits of the cuticle. To our knowledge, this is the first time that the composite profile of the cuticle has been related to a gradient in elasticity and tensile performance across a cuticular structure in arthropods. Because these associations were independent of species membership, we posit that the behavior of the cuticle is consistent across the genus, and that rostral flexibility is achieved exclusively through a modified cuticle lay-up in all *Curculio* species. This conclusion raises the intriguing possibility that a single ancestral shift in cuticle organization at the rostral apex – yielding higher flexibility and tensile strength – opened a large region of morphospace for exploration, resulting in present day diversity of the genus.

Based on fractographic analysis of the test-specimens, we infer that the exocuticle exhibits brittle fracture at a comparatively low strain, due to shearing between the endocuticle macrofibers to which it is anchored; these macrofibers fail at higher strain as a result of mixed-mode shearing and tensile fracture within and between laminae. This outcome is consistent with behavior shown in previous studies and is congruent with theoretical consideration of cuticle microstructure in CLPT, which predicts extension shear-coupling ($A_{16}, A_{26} \neq 0$) for individual off-axis macrofiber laminae [31, 32]. These results imply that fracture initiation occurs in the comparatively brittle exocuticle, and that the reduction in exocuticle thickness in the snout apex might serve to mitigate crack formation in rostral bending. Based on this pattern of fracture behavior, we identified the exocuticle-rich occipital suture as a common point of void nucleation and crack initiation. From a biological perspective, these findings reveal an unexpected morphological source of evolutionary constraint on rostral flexibility, raising the intriguing possibility that this system evolved primarily via negative selection of fracture, rather than positive selection of flexibility. In particular, the cuticle is invaginated in precisely the portion of the snout that experiences the greatest degree of tension during antero-dorsal flexion; the doubly-thick exocuticle in the invagination thus creates an unavoidable, brittle weak-point in the otherwise endocuticle-dominated rostral apex. This constraint, as well as the minimization of exocuticle thickness in the rostral apex, and the increased toughness derived from a thickened endocuticle, lead us to consider the avoidance

437 of catastrophic structural failure as a driving selective 442 able in the online version of this paper.
 438 pressure in the evolution of the rostrum.

439

VI. METHODS

440 Methods, including statements of data availability and
 441 any associated accession codes and references, are avail-

443

REFERENCES

- [1] Jansen, M. A., Singh, S. S., Chawla, N., & Franz, N. M. A multilayer micromechanical model of the cuticle of *Curculio longinasus* Chittenden, 1927 (Coleoptera: Curculionidae). *J. Struct. Biol.* **195**: 2, 139–158, (2016).
- [2] Vincent, J. F. V. & Wegst, U. G. K. Design and mechanical properties of insect cuticle. *Arthropod Struct. Dev.* **33**:3, 187–199, (2004).
- [3] Hepburn, H. R. & Ball, A. On the structure and mechanical properties of beetle shells. *J. Mater. Sci.* **8**:5, 618–623, (1973).
- [4] van de Kamp, T. & Greven, H. On the architecture of beetle elytra. *Entomol. Heute* **22**, 191–204, (2010).
- [5] van de Kamp, T., Riedel, A. & Greven, H. Micromorphology of the elytral cuticle of beetles, with an emphasis on weevils (Coleoptera : Curculionoidea) *Arthropod Struct. Dev.* **45**:1, 14–22, (2015).
- [6] Neville, A. C., Parry, D. A. & Woodhead-Galloway, J. The chitin crystallite in arthropod cuticle. *J. Cell Sci.* **21**:1, 73–82, (1976).
- [7] Amini, S., Tadayon, M., Idapalapati, S., and Miserez, A. The role of quasi-plasticity in the extreme contact damage tolerance of the stomatopod dactyl club *Nat. Mater.* **14**:9, 943–950, (2015).
- [8] McCullough, E. L., Tobalske, B. W., and Emlen, D. J. Structural adaptations to diverse fighting styles in sexually selected weapons *Proc. Natl. Acad. Sci. USA* **111**:40, 14484–14488, (2014).
- [9] McCullough, E. L. Mechanical limits to maximum weapon size in a giant rhinoceros beetle *Proc. R. Soc. B* **281**, 20140696, (2014).
- [10] Dirks, J., Parle, E., and Taylor, D. Fatigue of insect cuticle *J. Exp. Biol.* **216**:10, 1924–1927, (2013).
- [11] Dirks, J. and Taylor, D. Fracture toughness of locust cuticle *J. Exp. Biol.* **215**:9, 1502–1508, (2012).
- [12] Singh, S. S., Jansen, M. A., Franz, N. M., and Chawla, N. Microstructure and nanoindentation of the rostrum of *Curculio longinasus* Chittenden, 1927 (Coleoptera: Curculionidae) *Mater. Charact.* **118**, 206–211, (2016).
- [13] Toju, H. and Sota, T. Imbalance of predator and prey armament: geographic clines in phenotypic interface and natural selection *Am. Nat.* **167**:1, 105–117, (2005).
- [14] Gibson, L. P. Monograph of the genus *Curculio* in the New World (Coleoptera: Curculionidae). Part I. United States and Canada *Misc. Publ. Entomol. Soc. Am.* **6**, 239–285, (1969).
- [15] Dennell, R. The structure and function of the mouth-parts, rostrum and fore-gut of the weevil *Calandra granaria* L. *Phil. Trans. R. Soc. Lond. B* **231**:581, 247–291,
- [492] (1942).
- [493] [16] Morimoto, K. and Kojima, H. Morphologic characters of the weevil head and phylogenetic implications (Coleoptera, Curculionoidea) *Esakia* **43**, 133–169, (2003).
- [494] [17] Ting, P. C. Feeding mechanisms of weevils, their function, and relationship to classification *Mon. Bull. Dep. Agric. State Calif.* **22**, 161–165, (1933).
- [495] [18] Ting, P. C. The mouth parts of the coleopterous group Rhynchophora *Microentomology* **1**, 93–114, (1936).
- [496] [19] Aguirre Uribe, L. A. *Biology of the immature stages of the pecan weevil Curculio caryae (Horn) and oviposition habits of the adult weevil* (Ph.D. thesis, Texas A & M University, 1978).
- [497] [20] Moffett, M. Life in a nutshell *Natl. Geogr. Mag.* **176**, 783–784, (1989).
- [498] [21] *International Code of Zoological Nomenclature* Fourth Edition. (The International Trust for Zoological Nomenclature, London, 1999).
- [499] [22] Longhai, L. et al. Microstructure and mechanical properties of rostrum in *Cyrtotrachelus longimanus* (Coleoptera: Curculionidae) *Anim. Cells Syst.* **21**:3, 199–206, (2017).
- [500] [23] Matsumura, Y., Kovalev, A. E., and Gorb, S. N. Penetration mechanics of a beetle intromittent organ with bending stiffness gradient and a soft tip, *Sci. Adv.* **3**:12, eaao5469, (2017).
- [501] [24] Nikolov, S. et al. Robustness and optimal use of design principles of arthropod exoskeletons studied by ab initio-based multiscale simulations. *J. Mech. Behav. Biomed. Mater.* **4**:2, 129–145, (2011).
- [502] [25] Nikolov, S. et al. Revealing the design principles of high-performance biological composites using Ab initio and multiscale simulations: The example of lobster cuticle. *Adv. Mater.* **22**:4, 519–526, (2010).
- [503] [26] Blackwell, J. and Weih, M. Structure of chitin-protein complexes: ovipositor of the ichneumon fly *Megarhyssa*. *J. Mol. Biol.* **137**:1, 49–60, (1980).
- [504] [27] Bouligand, Y. Twisted fibrous arrangements in biological materials and cholesteric mesophases. *Tissue Cell* **4**:2, 189–217, (1972).
- [505] [28] Vincent, J. F. V. *Structural biomaterials* (Halsted Press, New York, 1982).
- [506] [29] Cheng, L., Wang, L., & Karlsson, A. M. Mechanics-based analysis of selected features of the exoskeletal microstructure of *Popillia japonica*. *Mater. Res.* **24**:11, 3253–3267, (2009).
- [507] [30] Leopold, R. A., Newman, S. M., and Helgeson, G. A comparison of cuticle deposition during the pre-and post-eclosion stages of the adult weevil, *Anthonomus grandis* BOHEMAN (Coleoptera: Curculionidae) *Int. J. Insect*

- 543 *Morphol. and Embryol.*, **21:1**, 37–62, (1992).
- 544 [31] Reddy, J. N. *Mechanics of laminated composite plates*
545 and shells: theory and analysis (CRC Press, Philadel-
546 phia, 2004).
- 547 [32] Jones, R. M. *Mechanics of composite materials* (CRC
548 press, Philadelphia, 2014).
- 549 [33] Hughes, J. and Vogler, A. P. The phylogeny of acorn
550 weevils (genus Curculio) from mitochondrial and nuclear
551 DNA sequences: the problem of incomplete data *Mol.*
552 *Phylogenet. Evol.* **32:2**, 601–615, (2004).
- 553 [34] Bonal, R. et al. Diversity in insect seed parasite guilds at
554 large geographical scale: the roles of host specificity and
555 spatial distance *J. Biogeogr.* **43:8**, 1620–1630, (2016).
- 556 [35] Hughes, J. and Vogler, A. P. Ecomorphological adapta-
557 tion of acorn weevils to their oviposition site *Evolution*
558 **58:9**, 1971–1983, (2004).
- 559 [36] Bonal, R., Espelta, J. M., and Vogler, A. P. Complex se-
560 lection on life-history traits and the maintenance of varia-
561 tion in exaggerated rostrum length in acorn weevils *Oe-*
562 *cologia* **167:4**, 1053–1061, (2011).
- 563 [37] Klocke, D. & Schmitz, H. Water as a major modulator
564 of the mechanical properties of insect cuticle. *Acta Bio-*
565 *mater.* **7**, 2935–2942 (2011).
- 566 [38] Mihai, L. A. and Goriely, A. How to characterize a non-
567 linear elastic material? A review on nonlinear constitu-
568 tive parameters in isotropic finite elasticity *Phil. Trans.*
569 *R. Soc. Lond. A* **473:2207**, 20170607, (2017).
- 570 [39] Münster, S. et al. Strain history dependence of the
571 nonlinear stress response of fibrin and collagen net-
572 works *Proc. Natl. Acad. Sci. USA* **110:30**, 12197–12202,
573 (2013).
- 574 [40] Felsenstein, J. Phylogenies and the comparative method
575 *Am. Nat.* **125:1**, 1–15, (1985).
- 576 [41] Revell, L. J. Phylogenetic signal and linear regression on
577 species data *Methods Ecol. Evol.* **1:4**, 319–329, (2010).
- 578 [42] Beament, J. W. L., Treherne, J. E., and Wigglesworth,
579 V. B. *Advances in insect physiology* Volume 4 (Academic
580 Press Inc., London, 1967).
- 581 [43] Sun, J. Y. et al. Differential constitutive equation of ely-
582 tra cuticle by nanoindentation *Adv. Mater. Res.*, **343**,
583 1133–1139, (2012).
- 584 [44] Greenhalgh, E. *Failure analysis and fractography of poly-*
585 *mer composites* (CRC press, Boca Raton, 2009).
- 586 [45] Davis, S. R. *Morphology, phylogeny, and evolutionary*
587 *development in the weevils (Insecta: Coleoptera: Cur-*
588 *culionoidea)* (Ph.D. thesis, University of Kansas, 2014).
- 589
- 602 tore Anzaldo for his assistance with histological staining.
- 603

AUTHOR CONTRIBUTIONS

604 M.A.J. conducted sectioning and staining, microscopy
605 and imaging, tensile and fatigue testing, statistical
606 analysis, and participated in manuscript preparation.
607 J.W. conducted tensile and fatigue testing and partic-
608 ipated in manuscript preparation. N.C. facilitated mi-
609 croscopy, tensile and fatigue testing, and participated
610 in manuscript preparation. N.M.F. facilitated specimen
611 acquisition and imaging and participated in manuscript
612 preparation.

ADDITIONAL INFORMATION

613 614 Supplementary information is available in the online
615 version of the paper. Reprints and permissions infor-
616 mation is available online at www.nature.com/reprints.
617 Correspondence and requests for materials should be ad-
618 dressed to M.A.J.

COMPETING FINANCIAL INTERESTS

619 620 The authors declare no competing financial interests.

ACKNOWLEDGMENTS

591 The authors are grateful to Robert Anderson (CMNC),
592 Lourdes Chamorro (USNM), and Charlie O'Brien
593 (CWOB) for their assistance and provision of specimens
594 used in this study. The authors thank Salvatore An-
595 zaldo, Andrew Johnston, Brian Reilly, Sangmi Lee, and
596 other ASUHIC members for their assistance in procur-
597 ing, treating, and maintaining specimen loans upon entry
598 into the ASUHIC. The authors would also like to thank
599 David Lowry (ASU CLAS Bioimaging Center) for his
600 training and assistance with resin embedding, scanning
601 electron microscopy, and microtomography, and Salva-

621

METHODS

622

Specimen acquisition and taxon sampling

623 Specimens for use in tensile and fatigue testing came
 624 from the Hasbrouck Insect Collection at Arizona State
 625 University [ASUC]. This set of specimens was supple-
 626 mented with material housed in the following collections,
 627 using the codens of Arnett et al. [46]:

628 CMNC: Canadian Museum of Nature Collection, Ottawa,
 629 Ontario, Canada

630 USNM: National Museum of Natural History, Washington,
 631 D.C., USA

632 Cold fracture, semi-thin sectioning, and tensile testing
 633 were conducted on randomly chosen female specimens
 634 belonging to six species obtainable through field work in
 635 the southwestern USA and northwestern Mexico. Taxon
 636 sampling was targeted to represent a mixture of disparate
 637 radiations and sister taxa with a variety of rostral mor-
 638 photypes, according to the phylogenetic hypotheses of
 639 Hughes et al. [33, 35] and Bonal et al. [34]. The six
 640 species of *Curculio* used herein are *C. caryae* (Horn,
 641 1873), *C. humeralis* (Casey, 1897), *C. proboscideus*
 642 Fabricius, 1775, *C. sulcatulus* (Casey, 1897), *C. uniformis*
 643 (LeConte, 1857), and *C. victoriensis* (Chittenden, 1904).

644

Histological sectioning

645 To illustrate the relative proportions of the cuticle re-
 646 gions in cross-section, serial semi-thin sectioning was con-
 647 ducted on exemplary female specimens of *C. humeralis*
 648 and *C. longinasus* Chittenden 1927. Live specimens of
 649 both species were collected into 95% ethanol for preser-
 650 vation. A female specimen was selected and the rostrum
 651 was separated from the head capsule with a fine-edged
 652 razor blade. The apical 1/4th of the rostrum was also
 653 removed and then discarded. The remaining portion of
 654 the rostrum and the head capsule were then embedded
 655 in EMbed812, as follows.

656 The cuticle was first immersed in acetone for 24 hours,
 657 and then transferred to a 2:1 mixture of acetone to epoxy
 658 resin. Samples remained at 21°C for 12 hours on a shaker
 659 table to prevent hardening. These were then transferred
 660 into a 1:1 mixture of acetone to resin, following by a
 661 1:2 mixture (each for 12 hours and at 21°C on a shaker
 662 table), before finally being placed into a silicone mold
 663 with pure resin. The mold was placed into an oven heated
 664 to 38°C, and the resin was allowed to cure for 24 hours.
 665 The resulting blocks were machined to prepare the apical
 666 surface of each sample for microtomy.

667 A Leica Ultracut R Microtome and diamond knife were
 668 used to expose a cross-section (transverse plane) of the
 669 apical and basal portions of the rostrum and to remove
 670 excess material. Semi-thin sections (0.5 µm thick) were

671 kept and stained with toluidine-blue-borax for light mi-
 672 croscopy and imaging.

673

Cold-fracture of specimens

674 Two pinned female specimens of each species were se-
 675 lected at random and retained for cold-fracturing of the
 676 rostrum. The heads of the specimens were removed and
 677 cleaned using a 95% ethanol solution and a thin paint-
 678 brush. Any muscles protruding from the occipital fora-
 679 men were removed with a fine-edged razor blade. The
 680 antennae were removed directly using forceps to pull the
 681 scape (basal section of antenna) from the antennal in-
 682 sertion. Cleaned specimens were stored at -80°C for 24
 683 hours, then fractured using forceps over a chilled alu-
 684 minum block. To fracture each specimen, the head cap-
 685 sule and rostrum were each gripped firmly in a pair of
 686 forceps; the forceps were then sharply rotated to fracture
 687 the base of the snout via dorsal flexion. The rostrum
 688 was fractured a second time, after separation from the
 689 head capsule, using the same procedure. The segmented
 690 specimens were then placed into individual glass vials to
 691 protect the fracture surfaces from contamination prior to
 692 microscopy.

693

Tensile and fatigue testing

694 *Force-controlled loading to failure* Five female spec-
 695 imens of each species were randomly allocated for use
 696 in tensile testing. The head of each specimen was re-
 697 moved, cleaned, and prepared as described above in the
 698 cold-fracture protocol. To avoid destroying the delicate,
 699 brittle specimens when gripping the ends of each head,
 700 a method was devised to create solid handles that could
 701 be clamped tightly into grips without risk of damage to
 702 the cuticle.

703 For each head, four 1 cm² strips of gaffer tape were cut;
 704 these were used as gripping and mounting points for the
 705 specimen. A strip of tape would be laid flat, with a large
 706 drop of cyanoacrylate glue placed upon the upturned sur-
 707 face. The curved portion of the snout was then placed
 708 into the drop such that the straight portion of the ros-
 709 trum was aligned perpendicular to the edge of the strip.
 710 Hardening of the cyanoacrylate effectively embedded the
 711 curved portion of the snout in a solid mass, isolating a
 712 straight section of the snout (from the base to a point
 713 distad of the apex of the scrobe) for testing. A second
 714 strip of tape was fixed over this mass with an additional
 715 layer of cyanoacrylate to provide a dorsal gripping sur-
 716 face for the mass, and a small mark was made to indicate
 717 the extent of the head inside the mass. This embedding
 718 procedure was likewise repeated for the head capsule, re-
 719 sulting in a finished specimen with anterior and posterior
 720 handles for testing.

721 Prior to testing, each specimen was placed in de-
 722 ionized water for 24 hours to allow full saturation of the

723 cuticle, simulating the condition of live tissue (see [37]).
 724 Once removed for testing, the specimen was gripped us-
 725 ing the cyanoacrylate handles at the marked locations
 726 immediately beyond the anterior margin of the rostrum
 727 and the posterior margin of the head capsule. The exposed
 728 section of the snout was coated in petroleum jelly using a
 729 cotton swab to prevent loss of moisture and stiffening of
 730 the specimen during the test. Specimens were loaded in
 731 a Tryton 250 Microforce Testing System equipped with
 732 a 5N load cell and mechanical clamp grip. All specimens
 733 were subjected to force-controlled uniaxial tension at a
 734 rate of $1.0 \text{ gf} \cdot \text{s}^{-1}$ until failure, with a sampling interval
 735 of 0.1 s. Engineering stresses ($\sigma_0 = F/A_0$) and strains
 736 ($\epsilon_0 = \Delta l/l_0$) were reported only for specimens that did
 737 not fracture due to strain accumulation at the interface
 738 between the rostrum and the cyanoacrylate handles.

739 *Displacement-controlled cyclic loading* To confirm
 740 that repeated, complete extension of a strongly curved
 741 rostrum would not result in fracture of the cuticle, a rep-
 742 resentative female specimen of *C. caryae* was allocated
 743 for fatigue testing. The head capsule of the specimen was
 744 fixed to a push-pin using cyanoacrylate glue; this served
 745 as a pedestal and gripping location for the posterior por-
 746 tion of the specimen. The apex of the rostrum was fixed
 747 to a strip of ripstop nylon fabric equal in length to the
 748 head using cyanoacrylate glue. As with tensile testing,
 749 the specimen was placed in de-ionized water for 24 hours,
 750 then coated in petroleum jelly using a cotton swab im-
 751 mediately prior to load cycling.

752 The end of the fabric was gripped and used to elon-
 753 gate the snout in tension by pulling on the fabric, thus
 754 isolating the effect of tension on the fatigue life of the ro-
 755 stral cuticle. In this way, the rostrum would return to its
 756 original configuration in a spring-like manner, as in liv-
 757 ing specimens, rather than being forced to return to the
 758 initial position. The snout was aligned such that com-
 759 plete elongation of the curved section would take place in
 760 tension with minimal off-axis deflection of the un-curved
 761 section. The specimen was subjected to displacement-
 762 controlled loading sufficient to fully extend the snout and
 763 generate a load stress of 1 N, or approximately 20% of the
 764 tensile strength of the species average. Load cycling took
 765 place at a rate of 0.33Hz, and was continued for 14 days
 766 (ca. 400K cycles), until the tensile stress in the sample
 767 approached an asymptotic minimum.

768 Once the test was concluded, the specimen was placed
 769 in a 50% ethanol solution for 24 hours to clean the
 770 petroleum jelly from the rostrum. The specimen was
 771 examined for surface fractures and micro-tears, then sub-
 772 jected to tensile testing via the same protocol as the other
 773 specimens to assess whether the cuticle had begun to fa-
 774 tigue.

775 Specimen imaging and microscopy

776 The fracture surfaces of cold-fractured specimens were
 777 examined using scanning electron microscopy to charac-

778 terize the composite profile and microstructure of the ro-
 779 strum. Fracture behavior of tensile testing specimens was
 780 assessed using both light microscopy and SEM to im-
 781 age the fracture surfaces of the specimens in transverse
 782 view. Electron microscopy was conducted using a JEOL
 783 JSM6300 scanning electron microscope, while light mi-
 784 croscopy was conducted using a Leica M205 C stereomi-
 785 croscope and attached computer running the software Le-
 786 ica Application Suite (LAS), as well as a Visionary Dig-
 787 ital Passport II system using a Canon EOS Mark 5D II
 788 camera outfitted with interchangeable macroscopic lenses.
 789 Specimen length, layer thicknesses, macrofiber orienta-
 790 tion angles, and cross-sectional areas were assessed in the
 791 Leica Application Suite and in Adobe Illustrator using
 792 pixel-wise measurements multiplied by a scaling factor
 793 for the image.

794 Constitutive modeling of the cuticle

795 *General Approach* The effective uni-axial membrane
 796 and transverse flexural elastic moduli of idealized cuti-
 797 cle organizations representing both the rostral apex and
 798 head capsule were estimated using Classical Laminate
 799 Plate Theory (CLPT); for general approach see [31, 32]).
 800 The composite profiles of both types of cuticle were ide-
 801 alized using the layer thicknesses and stacking sequences
 802 observed in *C. longinasus*. This particular species was
 803 chosen because we derived the effective elastic constants
 804 of the individual components of the cuticle in previous
 805 work [1, 12]. In addition, *C. longinasus* exhibits a profile
 806 that is typical and representative for the genus *Curculio*,
 807 based on examination of the six species used for tensile
 808 testing, as described previously.

809 For *C. longinasus* the total thickness of the cuticle
 810 in the head and rostrum is roughly 50 μm , as in most
 811 specimens of the other examined species. In the head
 812 capsule, the exocuticle occupies between 30-50% of
 813 the through-thickness of the laminate, with the re-
 814 maining thickness nearly evenly divided between 12
 815 layers of endocuticle. We use the maximum (50%
 816 of through-thickness, or 25 μm) for the model, since
 817 the cuticle appears to deviate from this value only
 818 in sulci (grooves), pores, and other scattered features
 819 of surface sculpture. The macrofiber laminae of the
 820 endocuticle were assigned a stacking sequence sequence of
 821 $0^\circ, 90^\circ, 30^\circ, -60^\circ, 60^\circ, -30^\circ, 90^\circ, 0^\circ, -60^\circ, 30^\circ, -30^\circ, 60^\circ$,
 822 thereby representing pairs of orthogonal plies stacked at
 823 a constant rotation angle of 30° , in approximation of the
 824 living tissue.

825 In the rostral apex, the exocuticle is reduced to a thin
 826 shell approximately 5 μm in thickness, or 10% of the total
 827 cuticle thickness. The endocuticle displays a more com-
 828 plex pattern of layer thicknesses in the rostral apex than
 829 in the head capsule. Each of the eight outermost lay-
 830 ers are of nearly equal thickness to the exocuticle (5 μm),
 831 while the four innermost layers have a combined thick-
 832 ness equal to that of the exocuticle or a single layer of

833 outer endocuticle ($h_{outer} = 5 \mu\text{m}$, $h_{inner} = 1.25 \mu\text{m}$). The
 834 stacking sequence with respect to the longitudinal axis
 835 of the rostrum forms an antisymmetric [$\pm 45^\circ$] angle-ply
 836 laminate.

837 To assess the individual contributions of layer thickness
 838 and stacking angle sequence to cuticle flexibility in the
 839 rostral apex, two hypothetical cuticle lay-ups were also
 840 modeled, each with only one of the modifications present
 841 in the cuticle of the rostral apex. The first of these models
 842 has the layer thicknesses of the rostral apex, but fiber
 843 orientations of the head capsule, while the second has
 844 the fiber orientations of the rostral apex, but the layer
 845 thicknesses of the head capsule.

846 Because these laminates are not symmetric, there ex-
 847 ist for each a bending-extension coupling matrix [B]
 848 populated with non-zero terms, thus complicating the
 849 calculation of effective in-plane elastic moduli. To cir-
 850 cumvent this difficulty and enable meaningful compari-
 851 son between each laminate, all of the layups are reflected
 852 about their inner surface. This effectively doubles their
 853 thickness while producing a balanced, symmetric lami-
 854 nate with no coupling between bending and extension
 855 (i.e., $[B] = 0_{3,3}$). Estimation of in-plane elastic constants
 856 from the extension([A]) and bending ([D]) matrices is de-
 857 scribed in detail below; Matlab R2018b was used to nu-
 858 merically evaluate the final values of the effective elastic
 859 constants [47].

860 *Classical Laminate Plate Theory* We begin by calcu-
 861 lating the 2D reduced stiffness matrix for each part of the
 862 cuticle. For orthotropic materials with the principal axes
 863 parallel to the ply edges, the reduced stiffness matrix is
 864 defined as follows:

$$[Q] = \begin{bmatrix} Q_{11} & Q_{12} & 0 \\ Q_{21} & Q_{22} & 0 \\ 0 & 0 & Q_{66} \end{bmatrix}, \quad (1)$$

865 and where:

$$\begin{aligned} Q_{11} &= \frac{E_1}{1 - \nu_{12}\nu_{21}}, \\ Q_{12} &= \frac{E_1\nu_{21}}{1 - \nu_{12}\nu_{21}} = Q_{21}, \\ Q_{21} &= \frac{E_2\nu_{12}}{1 - \nu_{12}\nu_{21}} = Q_{12}, \\ Q_{22} &= \frac{E_2}{1 - \nu_{12}\nu_{21}}, \\ Q_{66} &= G_{12}. \end{aligned} \quad (2)$$

866 For each layer k , the reduced stiffness matrix is trans-
 867 formed to account for the layer orientation angle θ within
 868 the laminate coordinate system, yielding a reduced trans-
 869 formed stiffness matrix according to:

$$[\bar{Q}] = [T]^{-1}[Q][T]^{-T}, \quad (3)$$

870 where the transformation matrix $[T]$ is defined as:

$$[T] = \begin{bmatrix} \cos^2 \theta & \sin^2 \theta & 2 \cos \theta \sin \theta \\ \sin^2 \theta & \cos^2 \theta & -2 \cos \theta \sin \theta \\ -\cos \theta \sin \theta & \cos \theta \sin \theta & \cos^2 \theta - \sin^2 \theta \end{bmatrix}. \quad (4)$$

871 Using the lay-ups specified for each type of cuticle
 872 described above, we calculate the extensional stiffness
 873 matrix $[A]$, bending stiffness matrix $[D]$, and bending-
 874 extension coupling matrix $[B]$ for each laminate consist-
 875 ing of n layers at a distance z from the laminate mid-
 876 plane. The elements of these matrices can be found ac-
 877 cording to:

$$\begin{aligned} A_{ij} &= \sum_{k=1}^n (\bar{Q}_{ij})_k (z_k - z_{k-1}), \\ B_{ij} &= \frac{1}{2} \sum_{k=1}^n (\bar{Q}_{ij})_k (z_k^2 - z_{k-1}^2), \\ D_{ij} &= \frac{1}{3} \sum_{k=1}^n (\bar{Q}_{ij})_k (z_k^3 - z_{k-1}^3). \end{aligned} \quad (5)$$

878 These stiffness matrices relate vectors of resultant
 879 forces $\{N\}$ and bending moments $\{M\}$ to mid-surface
 880 strains and curvatures $\{\epsilon^\circ\}$ and $\{\kappa\}$, respectively, in the
 881 laminate according to the following relationship:

$$\begin{Bmatrix} \{N\} \\ \{M\} \end{Bmatrix} = \begin{bmatrix} [A] & [B] \\ [B] & [D] \end{bmatrix} \begin{Bmatrix} \{\epsilon^\circ\} \\ \{\kappa\} \end{Bmatrix}. \quad (6)$$

882 For symmetric laminates, $[B] = 0_{3,3}$, and therefore:

$$\begin{aligned} \{N\} &= [A]\{\epsilon^\circ\}, \\ \{M\} &= [D]\{\kappa\}, \end{aligned} \quad (7)$$

883 or, in expanded form:

$$\begin{aligned} \begin{Bmatrix} N_{xx} \\ N_{yy} \\ N_{xy} \end{Bmatrix} &= \begin{bmatrix} A_{11} & A_{12} & A_{16} \\ A_{21} & A_{22} & A_{26} \\ A_{61} & A_{62} & A_{66} \end{bmatrix} \begin{Bmatrix} \epsilon_{xx}^\circ \\ \epsilon_{yy}^\circ \\ \gamma_{xy} \end{Bmatrix}, \\ \begin{Bmatrix} M_{xx} \\ M_{yy} \\ M_{xy} \end{Bmatrix} &= \begin{bmatrix} D_{11} & D_{12} & D_{16} \\ D_{21} & D_{22} & D_{26} \\ D_{61} & D_{62} & D_{66} \end{bmatrix} \begin{Bmatrix} \kappa_{xx} \\ \kappa_{yy} \\ \kappa_{xy} \end{Bmatrix}. \end{aligned} \quad (8)$$

884 If we make the simplifying assumptions (see [31, 32])
 885 that (1) the laminate experiences pure axial loading and
 886 transverse bending (i.e., $N_{yy} = N_{xy} = 0$ and $M_{yy} =$
 887 $M_{xy} = 0$, respectively) and (2) the laminate is a beam
 888 of sufficiently high aspect ratio to minimize the Poisson
 889 effect and anisotropic shear coupling (i.e., below we ef-
 890 fectively let $A_{12}^* = A_{16}^* = 0$ and $D_{12}^* = D_{16}^* = 0$), then
 891 we can calculate the in-plane effective flexural and axial
 892 Young's moduli of the laminate along the x-axis.

For axial Young's modulus of the laminate, we first define the average membrane stresses in the laminate as:

$$\{\bar{\sigma}^m\} = \frac{\{N\}}{z_1 - z_n}. \quad (9)$$

By substitution in Eq. 7, we find:

$$\begin{Bmatrix} \bar{\sigma}_{xx}^m \\ \bar{\sigma}_{yy}^m \\ \bar{\tau}_{xy}^m \end{Bmatrix} = \frac{1}{(z_1 - z_n)} \begin{bmatrix} A_{11} & A_{12} & A_{16} \\ A_{21} & A_{22} & A_{26} \\ A_{61} & A_{62} & A_{66} \end{bmatrix} \begin{Bmatrix} \epsilon_{xx}^m \\ \epsilon_{yy}^m \\ \gamma_{xy}^m \end{Bmatrix}, \quad (10)$$

and, by inverting this equation (let $A^* = A^{-1}$) and substituting $A_{12}^* = A_{16}^* = 0$ based on the assumptions above, we infer:

$$\epsilon_{xx}^m = (z_1 - z_n) A_{11}^* \bar{\sigma}_{xx}^m. \quad (11)$$

We therefore define Young's modulus for effective axial elasticity as:

$$E_{xx}^m = \frac{\bar{\sigma}_{xx}^m}{\epsilon_{xx}^m} = \frac{1}{(z_1 - z_n) A_{11}^*} \quad (12)$$

To find the transverse flexural Young's modulus of the laminate, we first specify the moment-curvature relation of an Euler-Bernoulli beam:

$$M = EI\kappa. \quad (13)$$

Along the x-axis, the second moment of area for a rectangular cross-section is:

$$I_{yy} = \frac{b(z_1 - z_n)^3}{12}, \quad (14)$$

Given the assumption that $M_{yy} = M_{xy} = 0$, the moment along the x-axis is related to the moment of the beam by:

$$M = M_{xx} b. \quad (15)$$

Thus, given the assumption that $D_{12}^* = D_{16}^* = 0$, Young's modulus for the effective transverse flexural elasticity of the laminate can be found by making Eq. 13 specific to transverse flexure of the x-axis and rearranging the terms:

$$E_{xx}^f = \frac{12M_{xx}}{(z_1 - z_n)^3 \kappa_{xx}} \quad (16)$$

From inversion of Eq. 7 (let $D^* = D^{-1}$) this reduces to:

$$E_{xx}^f = \frac{12}{(z_1 - z_n)^3 D_{11}^*} \quad (17)$$

Statistical analysis

Model selection and fitting In order to explore the relationships between the composite structure and mechanical properties of the cuticle, we fit phylogenetic linear mixed-effects models (PGLMM) to the tensile testing data using maximum likelihood estimation [48–51]. Raw data was processed using a custom script in Python version 3.5.2 [52]. Model exploration and fitting was conducted in R version 3.5.1 (2018-07-02) -- ‘Feather Spray’, using the ‘nlme’ and ‘ape’ packages [53–55]. Response variables and covariates were natural-log transformed, as needed, to ensure that the normalized model residuals were normally distributed [R:shapiro.test] and homoscedastic [R:levene.test], using numerical and graphical analysis (see Supplementary Data). In order to control for phylogenetic non-independence in the data, we included the species of each specimen as a random effect in all models. We also allowed for correlation in the error term of the models, as specified by a variance-covariance matrix generated from a Brownian motion [R:‘ape’:corBrownian] model of trait evolution along a phylogeny [54, 56].

The preferred phylogeny for North American *Curculio* is that of Bonal et al. [34]; this phylogeny was generated using Maximum-Likelihood methods and is untrametric, but has uniform internal branch lengths. The preferred tree was pruned to include only those species used in tensile testing, with a polytomy at each species to represent the individual specimens examined for that species; because the branch lengths of the tree were not specified, all branch lengths were set equal to 1. In general, phylogenetic regression is very robust with respect to missing or incomplete branch length data; underestimation of branch length causes overestimation of phylogenetic signal, which was not found to be statistically significant for any of our models, and we therefore believe that this procedure does not affect the findings of this study [56–58].

Other models of trait evolution were considered during model exploration, including Ornstein-Uhlenbeck [R:‘ape’:corMartins] and variable rate (AC/DC) [R:‘ape’:corBlomberg] models [54, 56]. However, neither of these produced a significantly better fit to the data than the Brownian motion model for any comparison, as measured by likelihood score and residual variance, viz. R_σ^2 and $R_{\beta^*}^2$ [R:‘r2glmm’:r2beta] (see Supplementary Data). R_σ^2 is the proportion of generalized variance explained by fixed effects, and is generally used to compare between covariance structures [59–61]. $R_{\beta^*}^2$ measures the multivariate association between the outcome and the fixed effects within a given correlation structure, and is generally used to compare between fixed effects [59–61]. We additionally estimated the phylogenetic signal in the residual variance of each model using two measures of spatial autocorrelation (Abouheif's C and Moran's I) and two measures of phylogenetic signal (Pagel's λ and Blomberg's κ) using the R package

973 ‘phytools’ [56, 62].

974 In all models, we tested whether the inclusion
 975 of phylogenetic correlation in the model error pro-
 976 duced significantly better model fit, using a likelihood-
 977 ratio test [`R::lmtest::lrtest`] and R^2_{σ} -difference
 978 test [`R::r2glmm::r2beta(method='sgv')`] between the
 979 fully-specified model and a model lacking the phylo-
 980 netic effect [61, 63]. Models that incorporated covariance
 981 due to Brownian motion consistently produced a higher
 982 likelihood score and fit to the data; however, no model ex-
 983 hibited statistically significant phylogenetic signal in any
 984 of the variables. Once models were fitted to the data,
 985 T and F-statistics were calculated to determine whether
 986 each cofactor was significantly different from zero.

987 *Hypothesis testing* Our objectives for hypothesis test-
 988 ing using the PGLMM’s were threefold: (1) assess
 989 whether the altered ratio of exocuticle to endocuticle in
 990 the rostral apex has an effect on the tensile strength of the
 991 snout; (2) test whether a trade-off exists between speci-
 992 men stiffness and resistance to fracture; and (3) examine
 993 whether snout length and flexibility are correlated.

994 To test the relationship between relative layer thick-
 995 nesses and tensile strength, we fitted a fully-specified
 996 model with the cross-sectional area of exocuticle and en-
 997 docuticle at the site of fracture as fixed effects, includ-
 998 ing an interaction term, and with maximum tensile force
 999 sustained prior to fracture as a response variable. This
 1000 model was then compared to models with only cross-
 1001 sectional area of either endocuticle or exocuticle, but not
 1002 both, as the sole fixed effect in the model. We then tested
 1003 the whether one or both regions was significantly cor-
 1004 related to the maximum force sustained in tension by
 1005 using likelihood-ratio tests and $R^2_{\beta^*}$ -difference tests be-
 1006 tween each of the three models. We found that only the
 1007 cross-sectional area of endocuticle was a significant fixed
 1008 effect, and therefore we elected to remove cross-sectional
 1009 area of exocuticle as a fixed effect to make the model
 1010 more parsimonious. The final model generated for our
 1011 first aim featured the ratio of exocuticle to endocuticle
 1012 in cross-section as a fixed effect, with ultimate tensile
 1013 strength as the response variable.

1014 For our second aim we examined the relationship be-
 1015 tween specimen stiffness and resistance to fracture. Speci-
 1016 men stiffness was characterized using a low strain elas-
 1017 tic modulus (averaged across the first 33% of the stress-
 1018 strain curve) and the secant modulus at failure. Re-
 1019 sistance to fracture was quantified in terms of ultimate
 1020 strain and fracture toughness (measured as area under
 1021 the stress-strain curve). Four models were fitted, two of
 1022 which had ultimate strain as the response variable and
 1023 two with fracture toughness as response variable. Each
 1024 model then used one of the different measures of speci-
 1025 men stiffness as a fixed effect.

1026 Finally, in the third aim we explored whether a size-
 1027 effect might exist in the *Curculio* rostrum, particularly
 1028 if longer (and typically more curved) rostra were more
 1029 flexible than shorter, straighter rostra. We generated two
 1030 models: the low strain and secant elastic moduli individ-
 1031 ually served as response variables, with specimen length
 1032 as the fixed effect in both.

Code availability

1033 R, Python, and Matlab scripts used to manipulate and
 1034 analyze the raw data (as well as their outputs), produce
 1035 figures, and estimate effective elastic constants is avail-
 1036 able from the corresponding author upon request.

1037 *Data availability*

1038 Stress-strain curves for all tensile and fatigue-tested
 1039 specimens are provided as PDFs (Supplement 1). Diag-
 1040 nostic plots for all PGLMMs are provided as PDFs (Sup-
 1041 plement 2). PGLMM terms and output are provided in
 1042 a PDF (Supplement 3). Raw and processed data will be
 1043 provided by the corresponding author upon reasonable
 1044 request.

1046

REFERENCES

- 1047 [46] Arnett Jr., R. H., Samuelson, G. A., and Nishida G. M. 1060 (2010).
- 1048 *The Insect and Spider Collections of the World, 2nd Edition*. Fauna and Flora Handbook No. 11. (Sandhill Crane 1061 Housworth, E. A., Martins, E. P., and Lynch, M.
 1062 The Phylogenetic Mixed Model *Am. Nat.* **163**:1, 84–96,
 1063 (2004).
- 1049 Press, Gainesville, 1993).
- 1050 [47] The MathWorks, Inc., *MATLAB and Statistics Toolbox* 1064 Stone, G. N., Sean, N., and Felsenstein, J. Controlling
 1051 (Natick, Mass., Release R2018b, 2018). 1065 for non-independence in comparative analysis of patterns
 1052 *Philos. Trans. Royal Soc. B* **366**:1569, 1410–1424, (2011).
- 1053 [48] Galecki, A. and Burzykowski, T. *Linear Mixed-Effects 1066*
 1054 *Models Using R*. A Step-by-Step Approach (Springer, 1067 Python Core Team. *Python: A dynamic, open source pro-
 1055 New York, 2013). 1068 gramming language* (Python Software Foundation, Ver-
 1056 [49] Hadfield, J. D. and Nakagawa, S. General quantita- 1069 sion 3.5.2, 2018).
- 1057 tive genetic methods for comparative biology: phyloge- 1070 [50] [53] R Development Core Team *R: A Language and Environ-
 1058 nies, taxonomies and multi-trait models for continuous 1071 ment for Statistical Computing* (R Foundation for Statisti-
 1059 and categorical characters *J. Evol. Biol.* **23**:3, 494–508, 1072 cal Computing, Vienna, Version 3.5.1, 2008).
- 1060 [54] Paradis, E. and Schliep, K. *ape 5.0: an environment 1073 for modern phylogenetics and evolutionary analyses in
 1074 1075*

- 1076 R *Bioinformatics* **5:0**, (2018).
- 1077 [55] Pinheiro, J. et al. nlme: Linear and Nonlinear Mixed 1090 effects models *Methods Ecol. Evol.* **4:2**, 133–142, (2013).
- 1078 Effects Models **R package version 3.1-137**, (2018).
- 1079 [56] Münkemüller, T. et al. How to measure and test phylo- 1091 [60] Jaeger, B. C., Edwards, L. J., Das, K., and Sen, P. K. 1092 An R² statistic for fixed effects in the generalized linear 1093 mixed model *J. Appl. Stat.* **44:6**, 1086–1105, (2016).
- 1080 genetic signal *Methods Ecol. Evol.* **3:4**, 743–756, (2012).
- 1081 [57] Stone, E. A. Why the phylogenetic regression appears 1094 [61] Jaeger, B. Computes R Squared for Mixed (Multilevel) 1095 robust to tree misspecification *Syst. Biol.* **60:3**, 245–260, 1096 Models **Version 0.1.2** (2017).
- 1082 (2011).
- 1083 [58] Molina-Venegas, R. and Rodríguez, M. Á. Revisiting 1097 [62] Liam, J. R. phytools: An R package for phylogenetic 1098 phylogenetic signal; strong or negligible impacts of poly- 1099 [63] Zeileis, A. and Hothorn, T. Diagnostic Checking in Re- 1100 tomies and branch length information? *BMC Evol. Biol.* 1100 **17:1**, 1–53, (2017).
- 1084 [59] Nakagawa, S. and Schielzeth, H. A general and simple 1098 method for obtaining R2 from generalized linear mixed- 1099 1100